

Wavefield simulations of earthquakes in Alaska for tomographic inversion

Vipul Silwal¹, Carl Tape¹ and Emanuele Casarotti²

¹Geophysical Institute and Department of Geosciences, University of Alaska Fairbanks, ²INGV, Rome, Italy

Email: {vsilwal, ctape}@alaska.edu



Overview

We assemble a catalog of moment tensors and a three-dimensional seismic velocity model for mainland Alaska, in preparation for an iterative tomographic inversion using spectral-element and adjoint methods. The catalog contains approximately 200 earthquakes with $M_w \geq 4.0$ that generate good long-period (≥ 6 s) signals for stations at distances up to approximately 500 km. To maximize the fraction of usable stations per earthquake, we divide our model into three subregions for simulations: south-central Alaska, central Alaska, and eastern Alaska. The primary geometrical interfaces in the model are the Moho surface, the basement surface of major sedimentary basins, and the topographic surface. The crustal and upper mantle tomographic model is from Eberhart-Phillips et al. (2006), but modified by removing the uppermost slow layer, then embedding sedimentary basin models for Cook Inlet basin, Susitna basin, and Nenana basin. We compute 3D synthetic seismograms using the spectral-element method. We demonstrate the accuracy of the initial three-dimensional reference model in each subregion by comparing 3D synthetics with observed data for several earthquakes originating in the crust and underlying subducting slab. Full waveform similarity between data and synthetics over the period range 6 s to 30 s provides a basis for an iterative inversion. The target resolution of the crustal structure is 4 km vertically and 20 km laterally. We use surface wave and body wave measurements from local earthquakes to obtain moment tensors that will be used within our tomographic inversion. Local slab events down to 180 km depth, in addition to pervasive crustal seismicity, should enhance resolution.

Source inversion

We perform a grid search in the moment tensor model space m = (strike, cos(dip), rake, M_w , depth). See Silwal and Tape (2016) for details on methodology and application to southern Alaska.

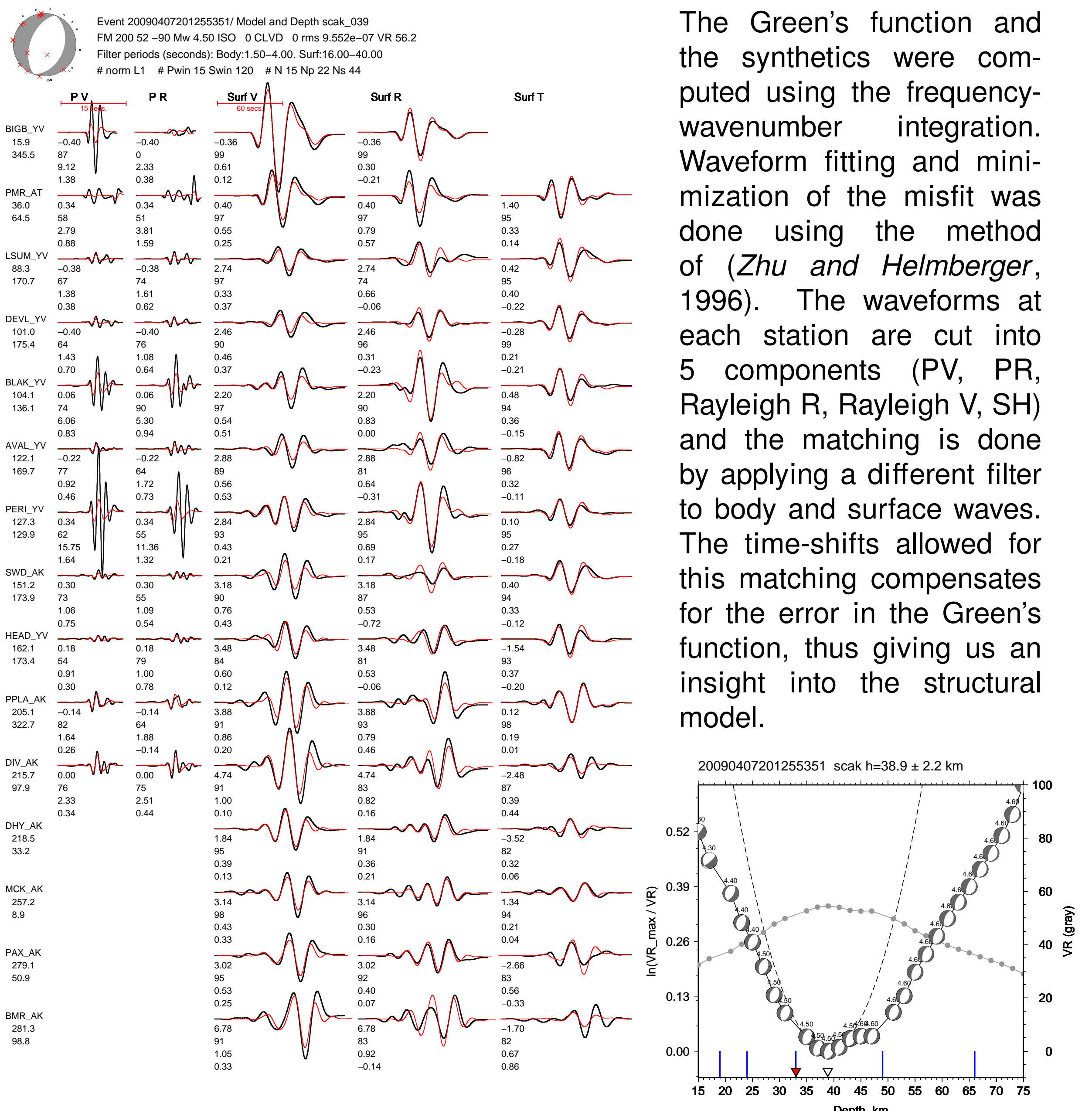


Figure 1: (left) Moment tensor solution and waveform comparisons for the example event in Anchorage, April 7, 2009. Waveform fit between the data (black) and the synthetics (red). Number below the waveforms are, from top to bottom, (1) time shift required for matching the synthetics with the data; (2) maximum cross-correlation percentage between data and synthetics; (3) the percentage of the total misfit; (4) log amplitude between data and synthetics in each window. Number below the station name are distance and azimuth. (right) Grid search for best fitting depth. Blue ticks mark the layer boundaries in the 1D model used in the inversion.

Simulation regions

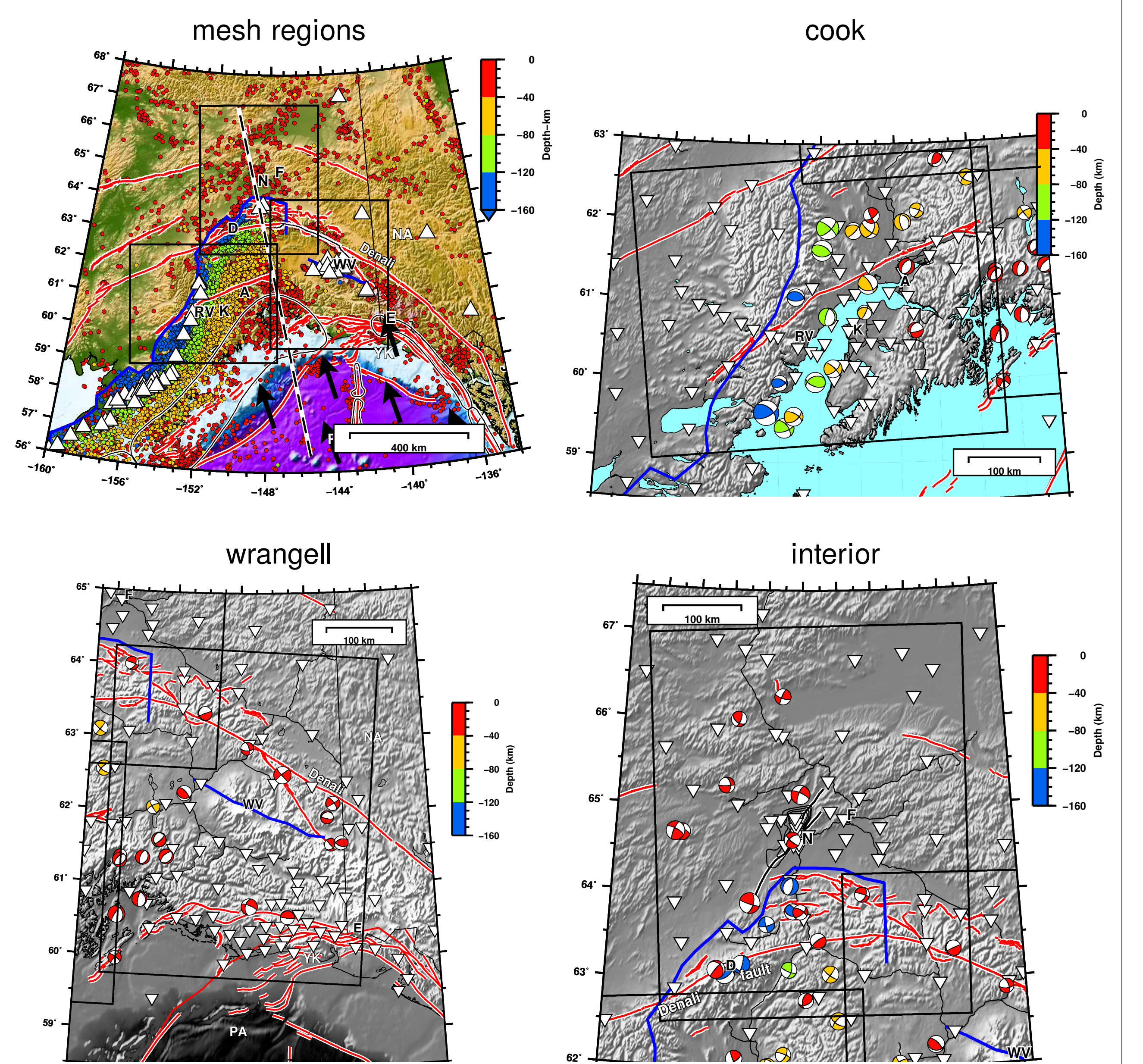


Figure 2: Simulations are performed in three different but overlapping meshes: **cook** (southern-central Alaska), **wrangell** (eastern Alaska), **interior** (central Alaska). All simulation domains are equal in dimension, 500 km x 400 km (Nelements = 535040). Topography is included in the mesh, and the model is extrapolated wherever necessary. The mesh includes 2 tripling layer at ~8 km and ~50 km, and extends to the depth of 400 km. We use 3D velocity model of Alaska obtained from Eberhart-Phillips et al. (2006) and embed local basins in it. For the 3D adjoint tomographic inversions this is our starting model. Moment tensors for earthquakes ($M_w \geq 4.0$) are estimated using methodology described in Figure 1.

Minimum resolvable period (NGLL test)

The minimum period (in seconds) that a mesh could resolve is obtained by comparing the waveforms obtained using coarse grid (NGLL=5) with those obtained using finer grid (NGLL=7).

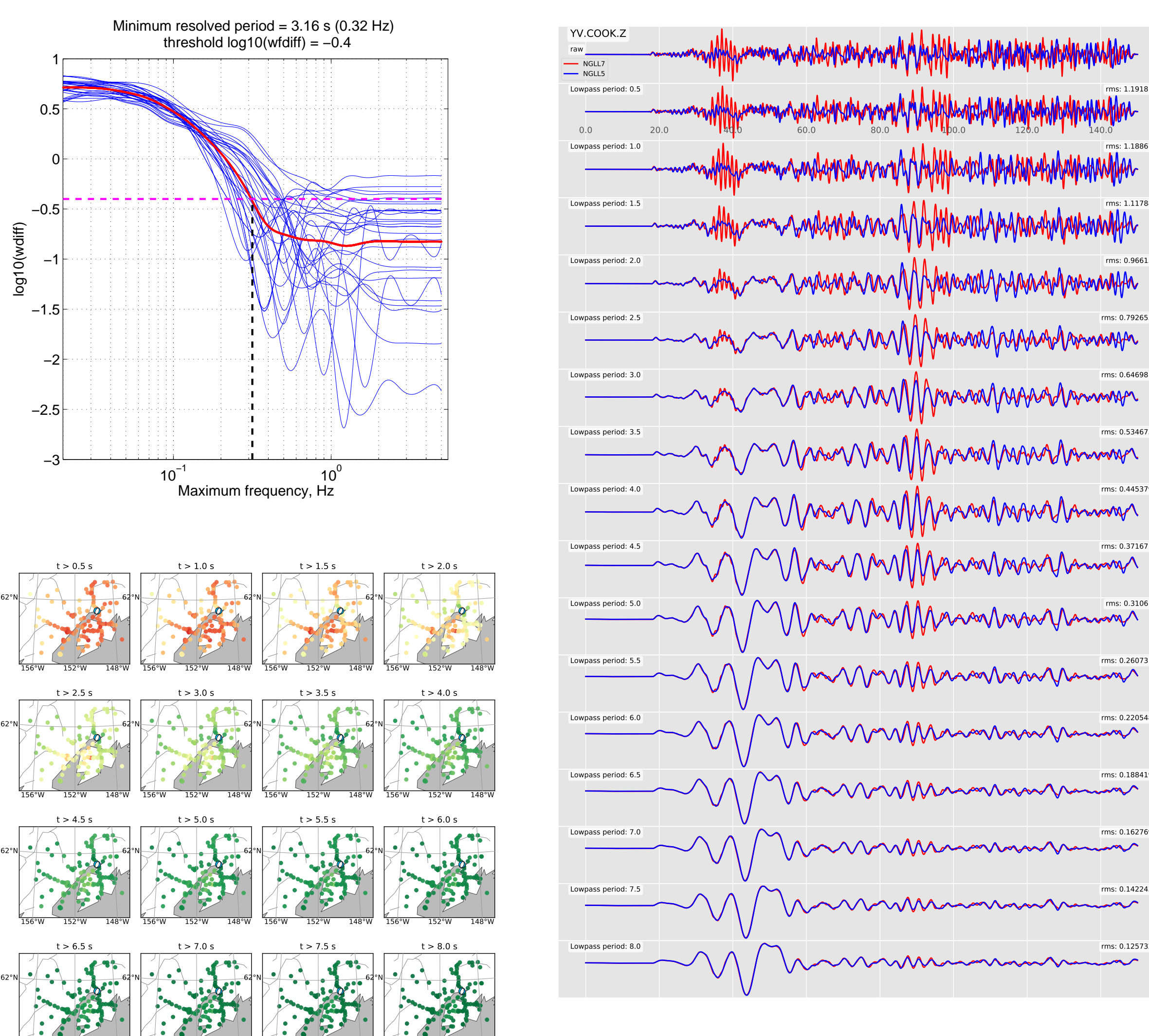


Figure 3: The minimum resolved period is obtained by thresholding the mean rms value across all stations at varying periods. (left) Plot of log10(period) vs Maximum frequency, Hz. (right) Grid search for best fitting depth. Blue ticks mark the layer boundaries in the 1D model used in the inversion.

Effect of smoothing topography

Using smoothed topography reduces the computational cost of simulations when using mesh with extreme topographic variations (example: wrangell mesh with Alaska range)

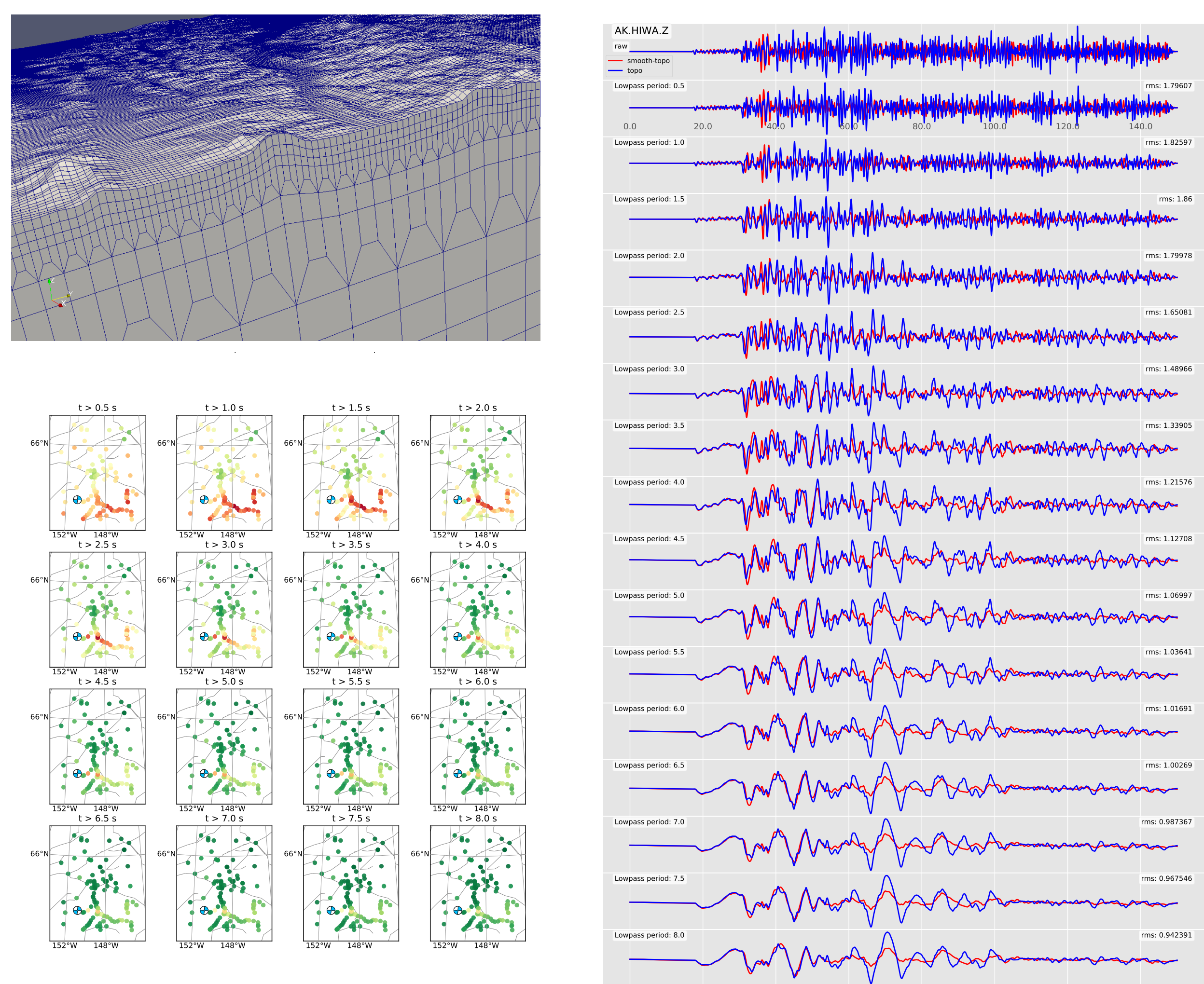


Figure 4: Effect of smoothing topography on the interior mesh. (bottom left) Map subplots shows that the rms misfit is significantly larger (in red) for the stations on the Alaska range. (right) Comparisons between waveforms generated using smoothed vs unsmoothed topo. The set of comparisons are of filtered waveforms for an example station at varying lowpass periods. Smoothed topography could be used instead of regular, if the waveform difference is insignificant above the minimum resolvable period.

Effect of including the basin

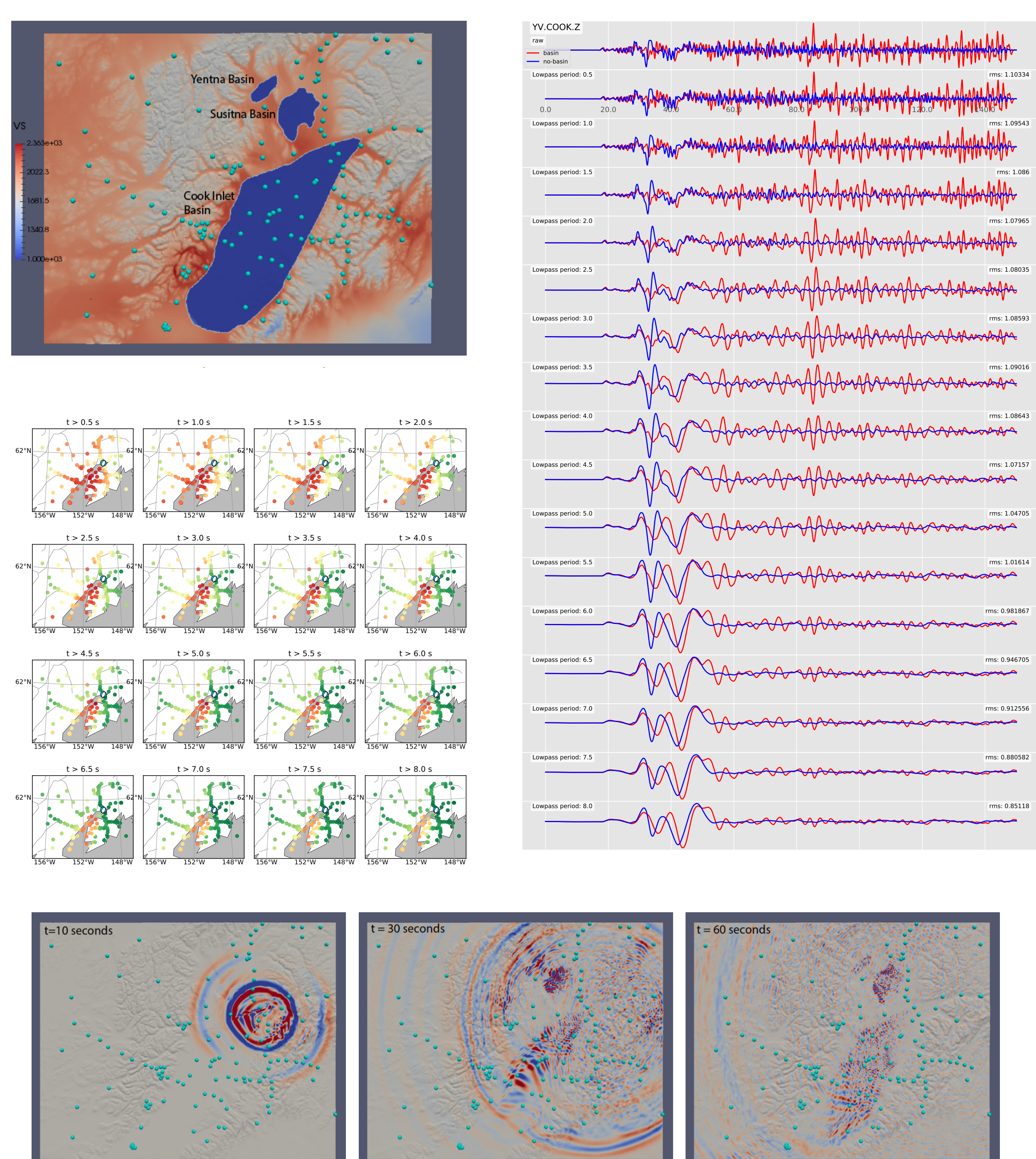


Figure 5: Effect of including basin on the seismic wavefields. Three basins are embedded into the velocity model: Cook Inlet, Susitna and Yentna basin. (left) Map subplots shows that the rms misfit is significantly larger at the basin station even at 8 seconds. (right) Comparisons between waveforms generated with basin vs without basin. (bottom) Snapshots of a 3D wavefield simulation showing the strong influence of the Cook Inlet basin on the wavefield. Blue circles denote permanent broadband stations.

Window selection and adjoint sources

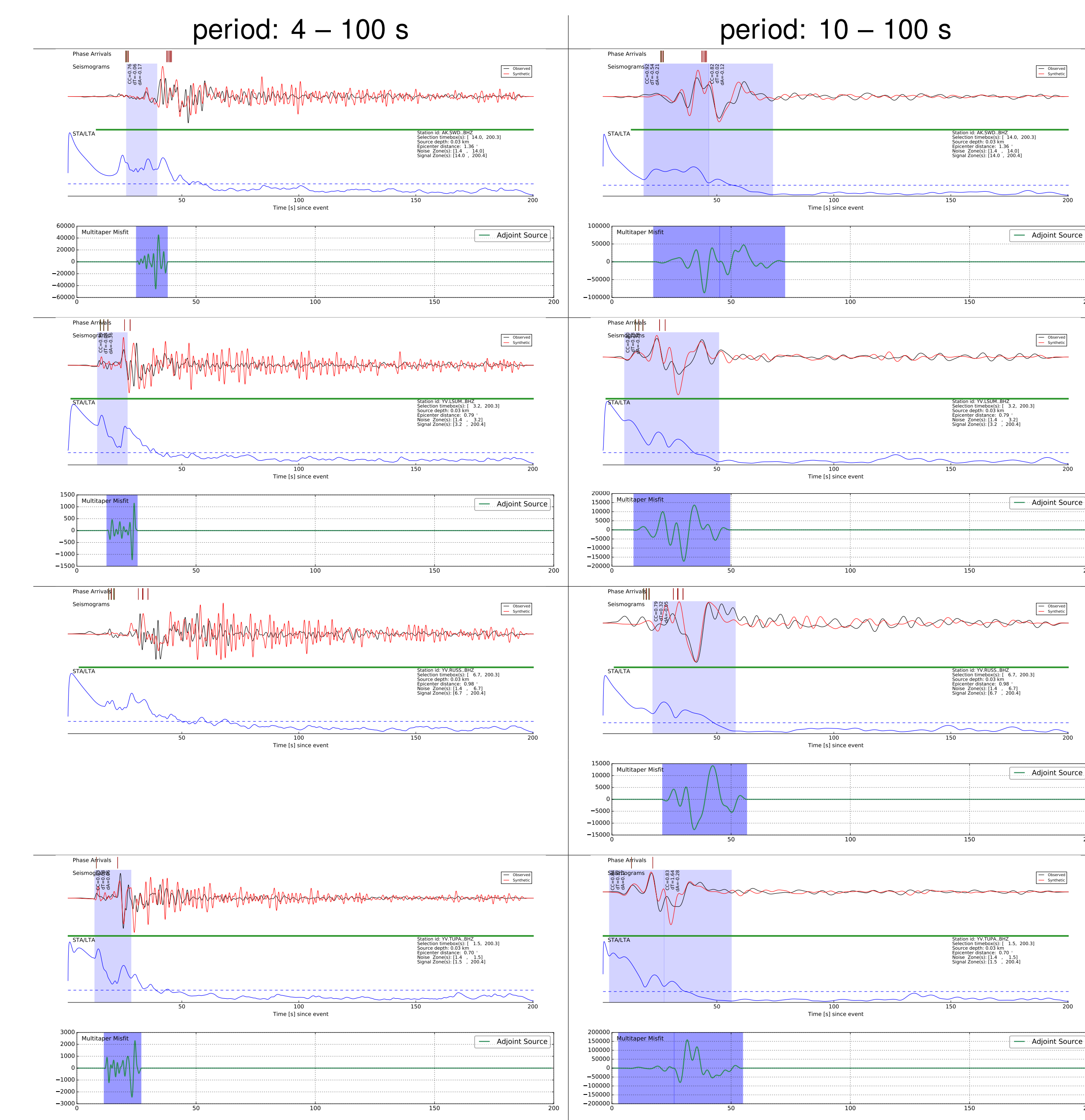


Figure 6: Both the observed and the synthetics are converted to asdf format prior to processing. Window selection is performed using pyflex (python version of FLEXWIN). Different bandpass filters are used to compute adjoint sources at short period and long period. Adjoint sources are computed using pyadjoint.

Summary

1. We perform moment tensor inversions in southern Alaska for 200 earthquakes between 2007-01-01 and 2016-06-01 (Silwal and Tape, 2016). The inversions were performed using body waves (1–3 s) and surface waves (16–40 s).
2. Wavefield simulation within a 3D earth structure model produce synthetic seismograms that differ significantly from 1D synthetics but are close enough to observed seismograms to allow us to quantify the waveform misfit and to use these differences within an adjoint tomographic inversion.
3. We examine the influence of the shallowest (slow) layers on 3D synthetic seismograms. It appears that the detailed model for Cook Inlet basin is necessary for achieving reasonable waveform fits, even at relatively long periods (>5 s).
4. We examine the effect of adding basin and topographic smoothing on seismic wavefields. Combined with the results from minimum resolvable period tests, it appears that we should not smooth topography and include basin with velocity thresholding ($v_{\text{min}} = 1000$ m/s).
5. Our next step is to calculate 3D synthetic seismograms for all earthquakes, then evaluate a misfit function, then calculate volumetric event kernels to be used within the tomographic inversion, following previous efforts such as in southern California (e.g., Tape et al., 2009).

Acknowledgments

We acknowledge support from NSF grant EAR-1215959. We would also like to thank Lion Krischer and Ryan Modrak for helping with data management and adjoint workflow.

References

- Eberhart-Phillips, D., D. H. Christensen, T. M. Brocher, R. Hansen, N. A. Ruppert, P. J. Haussler, and G. A. Abers (2006), Imaging the transition from Aleutian subduction to Yakutat collision in central Alaska, with local earthquakes and active source data, *J. Geophys. Res.*, 111, B11303, doi:10.1029/2005JB004240.
 Silwal, V., and C. Tape (2016), Seismic moment tensors and estimated uncertainties in southern Alaska, *J. Geophys. Res. Solid Earth*, 121, 2772–2797, doi:10.1002/2015JB012588.
 Tape, C., Q. Liu, A. Maggi, and J. Tromp (2009), Adjoint tomography of the southern California crust, *Science*, 325, 1175–1179, doi:10.1126/science.1175298.
 Zhu, L., and D. Helmberger (1996), Advancement in source estimation techniques using broadband regional seismograms, *Bull. Seismol. Soc. Am.*, 86(5), 1634–1641.